

# Dynamics-Level Watermarking of Flow Matching Models with Random Codes

Shuchan Wang

May 18, 2026

## Abstract

We introduce a dynamics-level approach to watermarking generative models. Rather than embedding signals into model weights or outputs, we embed the watermark directly into the learned continuous dynamics—the velocity field of a flow matching model. We formulate this as random coding over a continuous channel: a key-dependent perturbation is added during training, and the message is recovered at detection time from black-box queries. The perturbation is designed to leave the generated distribution unchanged. Experiments on MNIST and CIFAR-10 across different architectures confirm reliable message recovery, preserved generation quality, and chance-level decoding accuracy without the secret key.

## 1 Introduction

### 1.1 Background: Flow Matching Generative Models

Flow matching [7, 8] has emerged as a powerful framework for training continuous normalizing flows. Given samples  $x_1 \sim q_{\text{data}}$  from a data distribution and  $x_0 \sim p_{\text{noise}}$  from a simple base distribution, flow matching learns a time-dependent velocity field  $v_\theta(x, t)$  that transports  $p_{\text{noise}}$  to  $q_{\text{data}}$  along the trajectory

$$\frac{dx_t}{dt} = v_\theta(x_t, t), \quad t \in [0, 1]. \quad (1)$$

The model is trained by regressing  $v_\theta$  against a conditional velocity field  $u(x_t|x_0, x_1)$  defined along interpolating paths  $x_t = (1-t)x_0 + tx_1$ . At convergence, integrating the ODE from  $x_0 \sim p_{\text{noise}}$  produces samples  $x_1 \sim q_{\text{data}}$ .

The key object learned by flow matching is the velocity field  $v_\theta : \mathbb{R}^d \times [0, 1] \rightarrow \mathbb{R}^d$ , a continuous function that completely characterizes the generative process. Training such a model requires substantial computational resources, making the resulting velocity field valuable intellectual property in need of protection against unauthorized use.

### 1.2 Requirements for Generative Model Watermarking

A watermarking scheme for a generative model should satisfy the following properties. The watermark should be embedded in the model itself, so that it persists across different generated outputs and cannot be circumvented simply by bypassing a post-processing step (model-level embedding). Detection should require only query access to the model, without access to weights, training data, or the generation pipeline, enabling verification of deployed models accessible only through APIs (black-box verifiability). Watermarked

models should generate samples that are statistically indistinguishable from those of unwatermarked models, with no visible artifacts or degradation in fidelity (quality preservation). Detection and message recovery should require knowledge of a secret key; without the key, an attacker should be unable to recover the embedded message beyond chance level (keyed security). Finally, the scheme should support encoding a multi-bit message, enabling applications beyond binary ownership verification, including owner identification, model versioning, customer-specific serialization, and traitor tracing across distributed copies (multi-bit capacity).

### 1.3 Limitations of Existing Approaches

We categorize existing watermarking methods by what they watermark. Output-level methods embed signals into generated samples [10, 5]. These are not model-level: removing the post-processing step eliminates the watermark, and they provide no evidence of model ownership if the model itself is copied. Weight-level methods embed bits into model parameters [9]. While model-level, they require white-box access and are fragile to fine-tuning, pruning, or quantization. Behavior-level methods use backdoor triggers—specific inputs that produce predetermined outputs [1, 2, 4]. These methods operate at the model level and support black-box verification. However, trigger-based approaches can introduce visible artifacts or statistical irregularities, and often lack strong cryptographic keying: once a trigger is discovered, any party can verify the watermark. Recent work extends this to multi-bit payloads via channel coding [4].

Table 4 in Appendix C summarizes how existing paradigms compare against the five desiderata. To our knowledge, no prior work embeds the watermark directly into the learned continuous dynamics of the generative process itself. Existing black-box multi-bit methods instead rely on trigger behaviors, output statistics, or parameter-space embeddings, rather than perturbations of the transport dynamics.

### 1.4 The Gap: Dynamics-Level Watermarking

In flow matching, the velocity field  $v_\theta(x, t)$  is a continuous function that defines the generative dynamics. This perspective reveals an underexplored opportunity: the velocity field can be viewed as a high-dimensional continuous channel into which information may be embedded through structured perturbations, while preserving the overall behavior of the model.

This gap motivates our core question:

*Can we embed a verifiable, keyed, multi-bit message directly into the learned velocity field of a flow matching model, such that (1) the watermark is detectable with only black-box access, (2) generation quality is preserved, and (3) reliable detection requires access to a secret key?*

### 1.5 Our Approach and Contributions

Our specific contributions are as follows. First, we formulate watermarking directly at the level of the learned dynamics, embedding the message as a key-dependent perturbation of the continuous velocity field rather than into weights or outputs (model-level embedding). Second, we design the perturbation to integrate to zero over each generative trajectory, so that the terminal distribution of generated samples is preserved in practice (quality preservation). Third, the watermark is keyed by a secret projection matrix and an orthogonal codebook; without this key, empirical detection accuracy matches the random guess

### Training (Watermark Embedding)

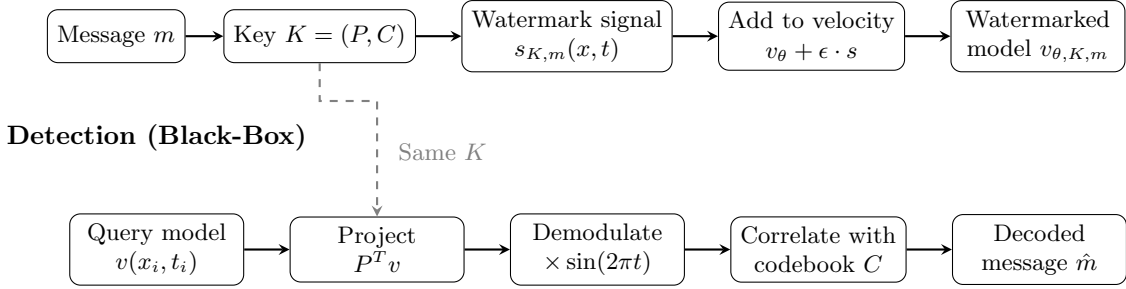


Figure 1: Overview of the proposed dynamics-level watermarking framework. **Top (Training):** A message  $m$  and secret key  $K$  define a time-modulated watermark signal  $s_{K,m}$ , which is added to the velocity field during flow matching. **Bottom (Detection):** Given black-box access to a model, the detector projects velocity queries into the code space, demodulates with the temporal carrier, and correlates against the codebook to recover the embedded message. The same key  $K$  is used for embedding and detection.

rate (keyed security). Fourth, the scheme supports multi-bit messages via the codebook construction, enabling identification beyond binary verification (multi-bit capacity). Fifth, we validate the method on MNIST and CIFAR-10 across MLP and UNet architectures, achieving 100% message recovery with chance-level false positive rate, FID ratios  $0.95 \times - 1.1 \times$ , and statistical separation exceeding  $8.4\sigma$  across all settings (empirical validation). These properties make dynamics-level watermarking a potential foundation for applications such as model ownership verification, traitor tracing, and regulatory compliance, though we leave their deployment-scale evaluation to future work.

## 2 Watermarking as Random Coding over Transport Dynamics

In this section, we formalize our approach. We first describe the information-theoretic motivation, then detail the construction of keys, codes, and the time-modulated watermark, followed by the training and detection procedures.

### 2.1 Information-Theoretic Motivation

From an information-theoretic perspective, our approach views the velocity field as a continuous additive channel. Let  $v_{\theta}(x, t)$  be the clean velocity field and consider a watermarked version:

$$v_{\theta, K, m}(x, t) = v_{\theta}(x, t) + \eta(x, t) + \epsilon \cdot s_{K, m}(x, t), \quad (2)$$

where  $\eta(x, t)$  represents background variation from training stochasticity and  $s_{K, m}(x, t)$  is a key-dependent signal encoding message  $m$ .

The detection problem becomes: given  $N$  noisy observations of  $v_{\theta, K, m}(x_i, t_i)$ , estimate  $\hat{m}$  with high confidence. This is a random coding problem over a continuous channel—a classical setup in information theory [3] that guarantees reliable decoding when the codebook is appropriately constructed and the number of observations is sufficient.

## 2.2 Message and Key: Framework

Equation (2) reduces the watermarking problem to the construction of the signal  $s_{K,m}(x, t)$ . We first give a general formulation.

Let  $m \in \mathcal{M}$  be a message from a set of  $|\mathcal{M}| := 2^L$  possible messages, and let  $K$  be a secret key. The key defines a codebook through a mapping

$$\phi_K : \mathcal{M} \rightarrow \mathcal{H}, \quad (3)$$

where  $\mathcal{H}$  is a function space over  $(x, t)$ . The codeword for message  $m$  is  $s_{K,m}(x, t) := \phi_K(m)$ .

The design of  $s_{K,m}$  must balance three considerations: (i) detectability—the signal must be recoverable from noisy observations through a known detection procedure; (ii) quality preservation—the signal must not alter the generated sample distribution, meaning it should integrate to zero along trajectories; and (iii) security—without knowledge of the key  $K$ , the watermark must be unrecoverable beyond chance level.

These considerations are formalized as the following three requirements on the codebook.

**Definition 1** (Admissible codebook). *A codebook  $\{s_{K,m}\}_{m \in \mathcal{M}}$  is called **admissible** if it satisfies the following conditions.*

1. **Zero-mean over time.** For all  $m \in \mathcal{M}$  and all  $x$ ,

$$\int_0^1 s_{K,m}(x, t) dt = 0. \quad (4)$$

2. **Approximate orthogonality.** For any distinct  $m, m' \in \mathcal{M}$ ,

$$\langle s_{K,m}, s_{K,m'} \rangle \approx 0. \quad (5)$$

3. **Energy normalization.** There exists a constant  $C > 0$  such that for all  $m \in \mathcal{M}$ ,

$$\|s_{K,m}\|^2 \approx C. \quad (6)$$

Condition 1 ensures the watermark integrates to zero along trajectories, preserving sample quality. Condition 2 ensures that different messages are maximally separable at detection time. Condition 3 ensures that all messages are equally detectable. These conditions are design principles that guide our construction; they are neither necessary for watermarking in general nor sufficient to guarantee empirical success. We validate the practical performance of our construction in Section 3.

## 2.3 Concrete Construction

We now present one construction satisfying Definition 1, chosen for its simplicity and exact satisfaction of the orthogonality condition. Other choices are possible, as discussed in Remark 1 below.

The secret key consists of two components,  $K = (P, C)$ . Here  $P \in \mathbb{R}^{D \times k}$  is a semi-orthogonal projection matrix satisfying  $P^T P = I_k$ , generated by QR decomposition of a random matrix seeded by  $K$ . This maps from the  $D$ -dimensional velocity space to a  $k$ -dimensional latent code space. The component  $C = \{c_m\}_{m \in \mathcal{M}}$  is a codebook of  $|\mathcal{M}| = 2^L$  unit vectors in  $\mathbb{R}^k$ , also generated via QR decomposition from  $K$ , such that each  $L$ -bit

message maps to a distinct codeword  $c_m$ . We require  $L \leq k$  so that pairwise orthogonal codewords can be assigned; in practice we use  $L < k$  and select  $2^L$  approximately orthogonal vectors from a random codebook, ensuring  $\langle c_m, c_{m'} \rangle \approx \delta_{m,m'}$  with high probability for sufficiently large  $k$ .

We define the watermark signal for message  $m$  as

$$s_{K,m}(x, t) = \sin(2\pi t) \cdot P c_m. \quad (7)$$

The signal separates naturally into a spatial component  $P c_m$ , which embeds the codeword into the velocity space, and a temporal carrier  $\sin(2\pi t)$ . The following theorem verifies that this construction satisfies all requirements.

**Theorem 1** (Verification of design properties). *The construction (7) satisfies the three conditions of Definition 1.*

*Proof.* We verify each condition.

1. **Zero-mean over time:**  $\int_0^1 s_{K,m}(x, t) dt = P c_m \int_0^1 \sin(2\pi t) dt = 0$ .
2. **Orthogonality:** Since  $P^T P = I_k$ , we have  $(P c_m)^\top (P c_{m'}) = c_m^\top c_{m'} = \delta_{m,m'}$ . With the temporal term,  $\langle s_{K,m}, s_{K,m'} \rangle = \mathbb{E}_t[\sin^2(2\pi t)] \cdot \delta_{m,m'} = \frac{1}{2} \delta_{m,m'}$ .
3. **Energy normalization:**  $\|s_{K,m}\|^2 = \frac{1}{2} \|P c_m\|^2 = \frac{1}{2}$  for all  $m$ , since  $P$  preserves norms and  $\|c_m\| = 1$ .

□

**Remark 1.** *This construction is one instance of a broader class. Alternative choices include different carrier functions (e.g.,  $\cos(2\pi t)$ ,  $\sin(4\pi t)$ , wavelet-based carriers), learned projections instead of random  $P$ , or sparse codes instead of orthogonal codes. Preliminary experiments with frequency- and time-division multiplexing did not improve capacity over the single-carrier design (see Appendix D); we leave a systematic investigation of multi-carrier schemes to future work.*

## 2.4 Watermarked Training

We now describe how the watermark is embedded during flow matching training. Given a training pair  $(x_0, x_1)$  and interpolated state  $x_t = (1-t)x_0 + tx_1$ , the standard flow matching target is  $u = x_1 - x_0$ . We modify this to include the watermark:

$$\tilde{v}(x_t, t) = u + \epsilon_0 \cdot s_{K,m}(x_t, t) = u + \epsilon_0 \sin(2\pi t) \cdot P c_m, \quad (8)$$

where  $\epsilon_0 > 0$  is the nominal perturbation amplitude applied during training. The effective watermark strength  $\epsilon$  in (2) may differ from  $\epsilon_0$ , because the  $\mathcal{L}_{\text{wm}}$  term in (9) provides an additional gradient that amplifies the effective  $\epsilon$ .

The watermarked model  $v_\theta$  is optimized with a combined objective:

$$\mathcal{L}(\theta) = \underbrace{\mathbb{E}_{x,t} [\|v_\theta(x, t) - \tilde{v}(x, t)\|^2]}_{\mathcal{L}_{\text{vel}}} + \lambda \cdot \underbrace{\mathbb{E}_{x,t} [-\sin(2\pi t) \cdot \langle P^T v_\theta(x, t), c_m \rangle]}_{\mathcal{L}_{\text{wm}}}, \quad (9)$$

where  $\lambda > 0$  balances the two terms. The first term  $\mathcal{L}_{\text{vel}}$  ensures the model learns the watermarked velocity field. The second term  $\mathcal{L}_{\text{wm}}$  directly rewards the model for producing velocity vectors whose demodulated projection aligns with the target codeword  $c_m$  (see Section 2.5). The following proposition shows how these two terms combine to determine the effective watermark strength.

**Proposition 1** (Optimal predictor under the watermark objective). *Assume expectations are finite and optimization is performed over all square-integrable vector fields  $v : \mathbb{R}^D \times [0, 1] \rightarrow \mathbb{R}^D$ . Then the unique population minimizer of (9) is*

$$v^*(x, t) = u(x, t) + \left( \epsilon_0 + \frac{\lambda}{2} \right) \sin(2\pi t) P c_m. \quad (10)$$

*Proof.* Since the objective is separable over  $(x, t)$ , it suffices to minimize the pointwise integrand

$$\ell(v) = \|v - \tilde{v}\|^2 - \lambda \sin(2\pi t) \langle P^T v, c_m \rangle. \quad (11)$$

Using the identity

$$\langle P^T v, c_m \rangle = \langle v, P c_m \rangle,$$

the gradient with respect to  $v$  is

$$\nabla_v \ell(v) = 2(v - \tilde{v}) - \lambda \sin(2\pi t) P c_m. \quad (12)$$

Setting the gradient to zero yields

$$v^* = \tilde{v} + \frac{\lambda}{2} \sin(2\pi t) P c_m. \quad (13)$$

Substituting

$$\tilde{v} = u + \epsilon_0 \sin(2\pi t) P c_m$$

gives

$$v^*(x, t) = u(x, t) + \left( \epsilon_0 + \frac{\lambda}{2} \right) \sin(2\pi t) P c_m. \quad (14)$$

Strict convexity of the quadratic term implies uniqueness.  $\square$

**Remark 2.** *Proposition 1 gives the population minimizer with effective watermark strength  $\epsilon_0 + \lambda/2$ . The empirical detection scores (Table 2) exceed this predicted value, which is expected: the parametric model  $v_\theta$  trained with finite data and stochastic optimization do not exactly recover the population optimum, and may allocate additional capacity to the watermark signal beyond the level predicted by the unconstrained population objective. Understanding this gap quantitatively is left to future work.*

## 2.5 Detection via Synchronous Demodulation

At detection time, we are given a model  $v$  (which may be watermarked or clean) and the secret key  $K = (P, C)$ . Detection requires only black-box query access to  $v$ .

We estimate the watermark signature via synchronous demodulation. Given  $N$  random query points  $(x_i, t_i)$ , the signature is computed as

$$\hat{s} = \frac{1}{N} \sum_{i=1}^N \sin(2\pi t_i) \cdot P^T v(x_i, t_i). \quad (15)$$

This estimator combines projection into the latent code space with synchronous demodulation of the temporal carrier. The multiplication by  $\sin(2\pi t_i)$  extracts the time-coherent component while averaging out background variation uncorrelated with the carrier, since  $\mathbb{E}[\sin(2\pi t)] = 0$ .

---

**Algorithm 1** Model Watermarking via Time-Modulated Random Coding

---

- 1: **Input:** Training pairs  $(x_0, x_1)$ , key  $K = (P, C)$ , message  $m$ ,
  - 2: watermark strength  $\epsilon_0$ , loss weight  $\lambda$
  - 3: Sample interpolation  $x_t = (1 - t)x_0 + tx_1$  and ground-truth velocity  $u = x_1 - x_0$
  - 4: Retrieve codeword  $c_m$  from codebook  $C$
  - 5: Define time-modulated watermark:  $s(x, t) \leftarrow \sin(2\pi t) \cdot Pc_m$
  - 6: Define watermarked training target:  $\tilde{v}(x_t, t) \leftarrow u + \epsilon_0 s(x_t, t)$
  - 7: Initialize model  $v_\theta$
  - 8: **for** each training step **do**
  - 9: Sample batch  $\{(x_t^{(i)}, t^{(i)}, \tilde{v}^{(i)})\}_{i=1}^B$
  - 10: Forward pass:  $\hat{v}^{(i)} \leftarrow v_\theta(x_t^{(i)}, t^{(i)})$
  - 11: Velocity loss:  $\mathcal{L}_{\text{vel}} \leftarrow \frac{1}{B} \sum_i \|\hat{v}^{(i)} - \tilde{v}^{(i)}\|^2$
  - 12: Project:  $z^{(i)} \leftarrow P^T \hat{v}^{(i)}$
  - 13: Demodulate:  $d^{(i)} \leftarrow \sin(2\pi t^{(i)}) \cdot z^{(i)}$
  - 14: Watermark loss:  $\mathcal{L}_{\text{wm}} \leftarrow -\frac{1}{B} \sum_i \langle d^{(i)}, c_m \rangle$
  - 15: Total loss:  $\mathcal{L} \leftarrow \mathcal{L}_{\text{vel}} + \lambda \mathcal{L}_{\text{wm}}$
  - 16: Update  $\theta$  via gradient descent
  - 17: **end for**
  - 18: **Output:** Watermarked model  $v_{\theta, K, m}$
- 

---

**Algorithm 2** Watermark Detection via Synchronous Demodulation

---

- 1: **Input:** Model  $v$  to test, key  $K = (P, C)$ , number of queries  $N$
  - 2: Sample  $N$  random points:  $(x_i, t_i) \sim \mathcal{N}(0, 4I_D) \times \text{Uniform}(0, 1)$
  - 3: Query model:  $y_i \leftarrow v(x_i, t_i)$  for  $i = 1, \dots, N$
  - 4: Project to code space:  $z_i \leftarrow P^T y_i \in \mathbb{R}^k$
  - 5: Demodulate with carrier:  $d_i \leftarrow \sin(2\pi t_i) \cdot z_i$
  - 6: Compute signature:  $\hat{s} \leftarrow \frac{1}{N} \sum_{i=1}^N d_i \in \mathbb{R}^k$
  - 7: Decode message:  $\hat{m} \leftarrow \arg \max_{m \in \mathcal{M}} \langle \hat{s}, c_m \rangle$
  - 8: **Output:** Decoded message  $\hat{m}$  and confidence score  $\max_m \langle \hat{s}, c_m \rangle$
- 

The embedded message is recovered by maximum-correlation decoding:

$$\hat{m} = \arg \max_{m \in \mathcal{M}} \langle \hat{s}, c_m \rangle. \quad (16)$$

With an approximately orthogonal codebook, this is equivalent to independent thresholding per bit.

The effectiveness of the detector follows from the structure of the watermark. Under a watermarked model, the demodulated signature concentrates around a scaled version of the embedded codeword; under a clean model, it remains near zero. A formal analysis of the expected response and convergence rate is provided in the proof of Theorem 2 (Appendix A). In summary,  $\mathbb{E}[\hat{s}] = \frac{\epsilon}{2} c_m$  for watermarked models and  $\mathbb{E}[\hat{s}] = 0$  for clean models, with estimation error  $O(1/\sqrt{N})$ .

## 2.6 Information-Theoretic Capacity

Our detection procedure can be analyzed as a communication channel.

**Theorem 2** (Capacity of the Demodulated Channel). *Consider the watermarked model with effective watermark strength  $\epsilon$ , projection dimension  $k$ , and key  $P$ . After synchronous*

demodulation and averaging over  $N$  independent queries, the extracted signature  $\hat{s}$  is approximately distributed according to the  $k$ -dimensional Gaussian channel

$$\hat{s} = \frac{\epsilon}{2}c_m + \xi, \quad \xi \sim \mathcal{N}(0, \Sigma_N), \quad (17)$$

where  $\Sigma_N = \Sigma/N$  and  $\Sigma$  is the covariance of  $\sin(2\pi t)P^T(v_\theta(x, t) + \eta_0(x, t))$  under the query distribution.

Under the Gaussian approximation and invertibility of  $\Sigma$ , the channel capacity is

$$\mathcal{C} = \frac{1}{2} \log \det \left( I_k + \frac{N\epsilon^2}{4} \Sigma^{-1} \right). \quad (18)$$

For large query budgets  $N$ , the capacity scales as

$$\mathcal{C} = \frac{k}{2} \log N + O(1), \quad (19)$$

showing that recoverable message information increases linearly with the projection dimension  $k$  and logarithmically with the number of detection queries.

*Proof.* See Appendix A. □

This result formalizes the scaling behaviour of the channel: capacity grows linearly with the projection dimension  $k$  and logarithmically with the number of queries  $N$ . We note two caveats. First, the Gaussian approximation relies on large  $N$  and independent queries; a rigorous finite-sample analysis is left to future work. Second, the linear growth in  $k$  suggests that capacity could be increased via frequency- or time-division multiplexing, but our preliminary experiments (Appendix D) found that such approaches reduce per-carrier signal strength and degrade detection accuracy.

We emphasize that the capacity analysis itself does not assume orthogonal codewords; it applies to any codebook. The orthogonal constraint arises from our specific construction (Definition 1, condition 2), which limits the codebook to  $k$  vectors and the message to  $\log_2 k$  bits. Our experiments with  $k = 32$  and  $L = 5$  bits operate at this limit. Scaling to larger message spaces requires either increasing  $k$  or relaxing the orthogonality constraint to allow approximately orthogonal codes, which the capacity analysis suggests would be effective but which we leave to future work.

## 2.7 Security Analysis

The security of the watermarking scheme relies on the secrecy of the projection matrix  $P \in \mathbb{R}^{D \times k}$  and the codebook  $C = \{c_m\}_{m \in \mathcal{M}} \subset \mathbb{R}^k$ . We consider an attacker with black-box access to a single deployed model  $v_{\theta, K, m}$  containing an unknown message  $m$ . The attacker may query the model at arbitrary inputs  $(x_i, t_i)$ ,  $i = 1, \dots, N$ , and observe the velocity vectors  $y_i = v_{\theta, K, m}(x_i, t_i) \in \mathbb{R}^D$ .

The watermark is embedded as  $s_{K, m}(x, t) = \sin(2\pi t) \cdot P c_m$ , where  $P$  maps the  $k$ -dimensional latent code space into the  $D$ -dimensional velocity space. An attacker without these components must recover them, or learn an equivalent decoding rule, from queries alone.

**Proposition 2** (Subspace search problem). *Given black-box query access to a single watermarked model  $v_{\theta, K, m}$ , recovering the watermark subspace  $\text{span}(P) \subset \mathbb{R}^D$  requires searching the Grassmann manifold  $Gr(k, D)$  of all  $k$ -dimensional subspaces in  $\mathbb{R}^D$ , which has dimension  $k(D - k)$ .*

*Proof.* From the observations  $y_i = v_\theta(x_i, t_i) + \eta(x_i, t_i) + \epsilon \sin(2\pi t_i) P c_m$ , the attacker can estimate the watermark component  $\sin(2\pi t) P c_m$  up to statistical noise. This reveals the action of  $P$  only through the vector  $P c_m \in \mathbb{R}^D$ , which lies in the  $k$ -dimensional subspace  $\text{span}(P)$ . To identify this subspace among all  $k$ -dimensional subspaces of  $\mathbb{R}^D$ , the attacker must solve a continuous optimization problem over the Grassmann manifold  $\text{Gr}(k, D)$ , whose dimension is  $k(D - k)$  [11].  $\square$

For our experimental parameters  $D = 784$  (MNIST) and  $k = 32$ , the search space has dimension  $32 \times 752 = 24,064$ . Subspace estimation from noisy linear measurements is a well-studied problem; the subsequent recovery of the correct basis and codebook introduces additional ambiguity, as shown below.

**Proposition 3** (Non-identifiability of the projection matrix). *Even if the attacker identifies the correct subspace  $\text{span}(P)$ , the projection matrix  $P$  is identifiable only up to an unknown orthogonal transformation of the latent code space. The original key pair  $(P, C)$  is not uniquely determined by the observations.*

*Proof.* Any matrix  $P' = PQ$  with orthogonal  $Q \in \mathbb{R}^{k \times k}$  spans the identical subspace and generates observationally equivalent watermark signals:  $\sin(2\pi t) P' (Q^T c_m) = \sin(2\pi t) P c_m$ . The pair  $(P', Q^T C)$  produces the same velocity field as  $(P, C)$ . Since infinitely many orthonormal bases span the same subspace, and each corresponds to a different latent codebook  $Q^T C$ , the original key pair  $(P, C)$  is underdetermined by the observations. An attacker who identifies the correct subspace still faces the problem of selecting the correct basis from among infinitely many candidates.  $\square$

Together, Propositions 2 and 3 characterize two obstacles to key recovery: identifying the watermark subspace requires search over a high-dimensional manifold, and even given the subspace, the projection matrix and codebook are not uniquely determined. A rigorous characterization of the sample and computational complexity of key recovery under our construction is left to future work.

Empirically, detection with an incorrect projection matrix  $P' \neq P$  yields 0/50 correct message recoveries on both MNIST and CIFAR-10, matching the random guess rate of  $1/|\mathcal{M}| \approx 3.1\%$  (Table 1). Clean models show no significant correlation with any codeword, confirming that the watermark signal does not arise from training artifacts.

## 3 Experiments

We evaluate our watermarking method on two image datasets: MNIST and CIFAR-10. We assess three key properties: (i) watermark detection accuracy, (ii) preservation of sample quality as measured by Fréchet Inception Distance (FID), and (iii) security against detection without the secret key.

### 3.1 Experimental Setup

We evaluate on two datasets: MNIST (grayscale,  $28 \times 28$ ) and CIFAR-10 (color,  $32 \times 32$ ). For MNIST, we use two architectures: a 4-layer MLP with 1,024 hidden units and SiLU activations, trained for both 5,000 and 10,000 steps to assess whether the watermark persists under extended training; and a UNet architecture with LoRA fine-tuning [6], where a clean UNet base model is trained for 5,000 steps and watermarks are embedded via low-rank adaptation matrices trained for 500 steps per message while base weights remain frozen. For CIFAR-10, we train a UNet architecture for 5,000 steps to obtain a

Table 1: Watermark detection performance across all models and datasets.

	Trials	Accuracy
<i>MNIST (MLP, 5K steps)</i>		
Watermarked models (6 total)	120	120/120 (100%)
Clean models (2 total)	40	0/40 (0%)
<i>MNIST (MLP, 10K steps)</i>		
Watermarked models (6 total)	120	120/120 (100%)
Clean models (2 total)	40	1/40 (2.5%)
<i>MNIST (UNet + LoRA)</i>		
Watermarked models (3 total)	60	60/60 (100%)
Clean model	60	0/60 (0%)
<i>CIFAR-10 (UNet + LoRA)</i>		
Watermarked models (3 total)	60	60/60 (100%)
Clean model	60	0/60 (0%)
<i>Wrong key attack (all datasets)</i>		
Random $P' \neq P$	50	0/50 (0%)
Random guess baseline	–	3.1% (1/32)

Table 2: Statistical separation and signature statistics.

Dataset / Architecture	WM Score	Clean Score	$\ \hat{s}\ $ (WM / Clean)	Min. Separation
MNIST (MLP, 5K)	0.58–1.11	−0.09–0.11	1.06 / 0.69	$8.4\sigma$
MNIST (MLP, 10K)	1.41–2.07	0.01–0.16	1.85 / 0.84	$25.5\sigma$
MNIST (UNet)	0.29–0.45	−0.07–0.15	0.66 / 0.56	$8.6\sigma$
CIFAR-10 (UNet)	0.62–0.64	−0.01–0.00	0.65 / 0.13	$17.9\sigma$

clean base model, then apply LoRA fine-tuning for 500 steps per message. The MLP on MNIST serves as a fast testbed; the UNet on both datasets demonstrates the method at a practical scale.

All experiments use projection dimension  $k = 32$  and 5-bit messages ( $L = 5$ , yielding  $|\mathcal{M}| = 32$ ). Detection uses  $N = 4,096$  random queries throughout. Complete hyperparameters are provided in Appendix F. We report detection accuracy, FID between generated and real samples, and the statistical separation between watermarked and clean models.

### 3.2 Watermark Detection

Table 1 summarizes detection performance. Across all architectures and training durations, watermarked models achieve 100% detection accuracy. On clean models, we observe zero false positives in all settings except the 10K-step MNIST MLP configuration, where one clean trial out of 40 produced a spurious detection (2.5%), which is below the random guess baseline of 3.1% and not statistically significant. An attacker using a random projection matrix instead of the true  $P$  achieves 0/50 accuracy, matching the random guess rate.

Table 3: Sample quality metrics across datasets and architectures. FID is computed against real test images (1,000 for MNIST; 10,000 for CIFAR-10).

Dataset / Architecture / Model	FID	FID Ratio
<i>MNIST (MLP, 5K steps)</i>		
Clean	7.4	–
WM Average	$8.1 \pm 0.3$	$1.10\times$
<i>MNIST (MLP, 10K steps)</i>		
Clean	7.3	–
WM Average	$6.9 \pm 0.1$	$0.947\times$
<i>MNIST (UNet + LoRA)</i>		
Clean	7.1	–
WM range	6.8–7.5	$0.955\times$ – $1.059\times$
<i>CIFAR-10 (UNet + LoRA)</i>		
Clean	24.3	–
WM range	23.5–25.1	$0.966\times$ – $1.032\times$

### 3.3 Statistical Separation

Table 2 reports per-message score statistics. Watermarked models consistently produce large positive scores, while clean model scores are near zero. The minimum separation across all settings is  $8.4\sigma$  (MNIST MLP), and all  $p$ -values are below  $10^{-37}$  (Welch’s  $t$ -test). These margins indicate that detection is robust to sampling variability and that false positives are highly unlikely under the observed statistics.

We additionally examine the signature norm  $\|\hat{s}\|$ , which measures the total signal energy in the projected space before correlating with any specific codeword. On MNIST,  $\|\hat{s}\|$  is comparable between watermarked and clean models across all architectures (e.g., 0.66 vs. 0.56 for UNet). On CIFAR-10, watermarked models exhibit a larger signature norm (0.65 vs. 0.13), meaning an attacker could potentially identify a model as watermarked by measuring the projected energy. We note that this does not compromise message recovery: without the codebook  $C$ , the attacker still cannot determine which message is embedded, and wrong-key decoding remains at chance level (Table 1). The watermark therefore satisfies the keyed security requirement: detection and message recovery require knowledge of the secret key.

### 3.4 Sample Quality Preservation

Table 3 quantifies sample quality. Across all settings, the FID ratio between watermarked and clean models remains close to  $1.0\times$ . We note that in several configurations watermarked models achieve marginally lower FID than the corresponding clean baseline (e.g., 6.9 vs. 7.3 at 10K steps). This is attributable to random training variation and finite-sample FID estimation noise. The key finding is that FID ratios remain tightly clustered around  $1.0\times$ , confirming that the watermark perturbation does not degrade sample quality. The generated samples are provided in Appendix E.

These results validate the design of the time-modulated perturbation: because it integrates to zero over each trajectory, sample quality is preserved in practice across datasets, architectures, and training durations.

## 4 Conclusion

We have presented a method for embedding verifiable, multi-bit messages directly into the learned dynamics of flow matching generative models. The watermark is a key-dependent perturbation of the velocity field, recovered through synchronous demodulation from black-box queries, and designed to integrate to zero over each trajectory so that generation quality is preserved.

Experiments across MNIST and CIFAR-10 with MLP and UNet architectures confirm 100% detection accuracy, FID ratios close to  $1.0\times$ , and chance-level detection without the secret key. Extending training to 10,000 steps does not degrade watermark recovery; a persistence analysis is provided in Appendix B.

Several directions remain open. A rigorous finite-sample analysis of the demodulated channel would sharpen the capacity guarantees. Extending the approach to other generative model families and evaluating robustness to model compression or fine-tuning are natural next steps. The dynamics-level perspective introduced here, treating the learned velocity field as a continuous communication channel, may also prove useful beyond watermarking.

**Code availability.** Code and experimental configurations are publicly available at: <https://github.com/ShuchanWang/flow-matching-dynamics-watermarking>.

## References

- [1] Yossi Adi et al. “Turning your weakness into a strength: Watermarking deep neural networks by backdooring”. In: *27th USENIX security symposium (USENIX Security 18)*. 2018, pp. 1615–1631.
- [2] Huili Chen, Bitan Darvish Rouhani, and Farinaz Koushanfar. “Blackmarks: Blackbox multibit watermarking for deep neural networks”. In: *arXiv preprint arXiv:1904.00344* (2019).
- [3] Thomas M Cover. *Elements of information theory*. John Wiley & Sons, 1999.
- [4] Jianwei Fei, Benedetta Tondi, and Mauro Barni. “High payload robust watermarking of generative models with multiple triggers and channel coding”. In: *The 1st Workshop on GenAI Watermarking*. 2025.
- [5] Pierre Fernandez et al. “The stable signature: Rooting watermarks in latent diffusion models”. In: *Proceedings of the IEEE/CVF International Conference on Computer Vision*. 2023, pp. 22466–22477.
- [6] Edward J Hu et al. “Lora: Low-rank adaptation of large language models.” In: *Iclr* 1.2 (2022), p. 3.
- [7] Yaron Lipman et al. “Flow Matching for Generative Modeling”. In: *The Eleventh International Conference on Learning Representations*.
- [8] Xingchao Liu, Chengyue Gong, et al. “Flow Straight and Fast: Learning to Generate and Transfer Data with Rectified Flow”. In: *The Eleventh International Conference on Learning Representations*.
- [9] Yusuke Uchida et al. “Embedding watermarks into deep neural networks”. In: *Proceedings of the 2017 ACM on international conference on multimedia retrieval*. 2017, pp. 269–277.

- [10] Yuxin Wen et al. “Tree-ring watermarks: Fingerprints for diffusion images that are invisible and robust”. In: *arXiv preprint arXiv:2305.20030* (2023).
- [11] Lizhong Zheng and David N. C. Tse. “Communication on the Grassmann manifold: A geometric approach to the noncoherent multiple-antenna channel”. In: *IEEE transactions on Information Theory* 48.2 (2002), pp. 359–383.

## A Proof of Theorem 2

We derive the capacity formula in three steps: establishing the effective channel model, characterizing the noise covariance, and applying the vector Gaussian channel capacity result. We state all assumptions explicitly.

### A.1 Step 1: Approximate Effective Channel

Given a watermarked model  $v_{\theta,K,m}$ , we query it at  $N$  random points  $\{(x_i, t_i)\}_{i=1}^N$  drawn i.i.d. from a sampling distribution  $p(x, t)$  and compute the signature:

$$\hat{s} = \frac{1}{N} \sum_{i=1}^N \sin(2\pi t_i) \cdot P^T v_{\theta,K,m}(x_i, t_i). \quad (20)$$

Decompose the velocity field as  $v_{\theta,K,m} = v_{\theta} + \eta_0 + \epsilon \sin(2\pi t) P c_m$ , where  $v_{\theta}$  is the learned flow,  $\eta_0$  represents background variation from training stochasticity and model approximation error, and  $\epsilon \sin(2\pi t) P c_m$  is the watermark signal. Substituting:

$$\hat{s} = \frac{1}{N} \sum_{i=1}^N \sin(2\pi t_i) P^T [v_{\theta}(x_i, t_i) + \eta_0(x_i, t_i)] \quad (21)$$

$$+ \frac{\epsilon}{N} \sum_{i=1}^N \sin^2(2\pi t_i) P^T P c_m. \quad (22)$$

Since  $P^T P = I_k$  by construction, the second term simplifies to:

$$\frac{\epsilon}{N} \sum_{i=1}^N \sin^2(2\pi t_i) \cdot c_m. \quad (23)$$

Define the background term for each query:

$$z_i := \sin(2\pi t_i) P^T [v_{\theta}(x_i, t_i) + \eta_0(x_i, t_i)] \in \mathbb{R}^k. \quad (24)$$

We introduce the following assumptions.

**Assumption 1** (Uncorrelated carrier and background). *The temporal carrier  $\sin(2\pi t)$  is uncorrelated with the background velocity field:*

$$\mathbb{E}_{x,t}[\sin(2\pi t) \cdot P^T (v_{\theta}(x, t) + \eta_0(x, t))] = 0. \quad (25)$$

Assumption 1 is justified because the carrier  $\sin(2\pi t)$  is a deterministic periodic function with zero mean over  $[0, 1]$ , while the background velocity field  $v_{\theta} + \eta_0$  is determined by the data distribution and training procedure, with no mechanism to correlate structurally with the carrier. Empirically, the near-zero clean-model scores in Table 2 support this assumption.

**Assumption 2** (Independent and identically distributed queries). *The query points  $\{(x_i, t_i)\}_{i=1}^N$  are drawn i.i.d. from a distribution  $p(x, t)$  under which the background terms  $z_i$  have finite second moments.*

Assumption 2 holds by construction, as queries are sampled independently. Under this assumption, the  $z_i$  are i.i.d. random vectors with mean  $\mathbb{E}[z_i] = \mathbf{0}$  (by Assumption 1) and covariance matrix

$$\Sigma := \text{Cov}(z_i) = \mathbb{E}[z_i z_i^T] \in \mathbb{R}^{k \times k}. \quad (26)$$

For the watermark term, we have:

$$\mathbb{E}[\sin^2(2\pi t)] = \int_0^1 \sin^2(2\pi t) dt = \frac{1}{2}. \quad (27)$$

By the Law of Large Numbers,  $\frac{1}{N} \sum_{i=1}^N \sin^2(2\pi t_i) \rightarrow \frac{1}{2}$  as  $N \rightarrow \infty$ .

For the background term, we apply the multivariate Central Limit Theorem (CLT). Let  $\xi := \frac{1}{N} \sum_{i=1}^N z_i$ . Under Assumptions 1 and 2, as  $N \rightarrow \infty$ :

$$\sqrt{N}\xi \xrightarrow{d} \mathcal{N}(0, \Sigma), \quad (28)$$

where  $\xrightarrow{d}$  denotes convergence in distribution. Equivalently, for large  $N$ :

$$\xi \approx \mathcal{N}\left(0, \frac{\Sigma}{N}\right). \quad (29)$$

**Assumption 3** (Gaussian approximation for finite  $N$ ). *For the query budgets  $N$  used in practice, the distribution of  $\xi$  is well-approximated by  $\mathcal{N}(0, \Sigma/N)$ .*

Assumption 3 is the strongest assumption. While the CLT guarantees asymptotic normality, the accuracy at finite  $N$  depends on the distribution of  $z_i$ . In practice,  $N \geq 10^3$  typically suffices for  $k \ll N$ ; our experiments use  $N = 4096$  with  $k = 32$ . We do not formally verify the Gaussian approximation and leave a rigorous finite-sample analysis to future work.

Combining the watermark and background terms, the effective channel for large  $N$  is:

$$\hat{s} = \frac{\epsilon}{2} c_m + \xi, \quad \xi \sim \mathcal{N}\left(0, \frac{\Sigma}{N}\right). \quad (30)$$

## A.2 Step 2: The Noise Covariance

The noise covariance  $\Sigma$  captures the background velocity variation in the projected  $k$ -dimensional space. Let  $u(x, t) := \sin(2\pi t)[v_\theta(x, t) + \eta_0(x, t)] \in \mathbb{R}^D$ . Then:

$$\Sigma = P^T \mathbb{E}_{x,t}[u(x, t)u(x, t)^T] P. \quad (31)$$

**Assumption 4** (Invertible covariance). *The projected covariance  $\Sigma$  is invertible.*

Since  $\mathbb{E}[uu^T]$  is a  $D \times D$  positive semidefinite matrix and  $P \in \mathbb{R}^{D \times k}$  is a random semi-orthogonal matrix with  $k \ll D$ ,  $\Sigma$  is invertible with high probability. Intuitively,  $P$  projects onto a random  $k$ -dimensional subspace, and the background velocity variation is sufficiently rich that its restriction to any such subspace has full rank. In our experiments,  $k = 32$  and  $D = 3072$  (CIFAR-10) or  $D = 784$  (MNIST), satisfying  $k \ll D$ .

### A.3 Step 3: Vector Gaussian Channel Capacity

Equation (30) describes a  $k$ -dimensional vector Gaussian channel with:

- Input:  $c_m \in \mathbb{R}^k$ , constrained to  $\|c_m\|^2 = 1$  (unit-norm codeword),
- Channel gain:  $\epsilon/2$ ,
- Additive noise:  $\xi \sim \mathcal{N}(0, \Sigma/N)$ .

Under the Gaussian approximation, this corresponds to an additive nonwhite Gaussian noise channel [3]. The capacity under an average power constraint  $\mathbb{E}[\|X\|^2] \leq P$  is:

$$\mathcal{C} = \max_{K_X: \text{tr}(K_X) \leq P} \frac{1}{2} \log \det (I_k + K_X K_Z^{-1}), \quad (32)$$

where  $K_Z = \Sigma/N$  is the noise covariance and  $K_X$  is the input covariance. The optimal  $K_X$  is obtained via water-filling over the eigenvalues of  $K_Z$ .

After scaling by  $2/\epsilon$ , the effective channel becomes

$$y = c_m + \xi', \quad \xi' \sim \mathcal{N}\left(0, \frac{4}{\epsilon^2 N} \Sigma\right). \quad (33)$$

Treating the watermark codewords as isotropically distributed unit-power inputs in  $\mathbb{R}^k$ , the corresponding Gaussian channel has effective capacity

$$\mathcal{C} = \frac{1}{2} \log \det \left( I_k + \frac{N\epsilon^2}{4} \Sigma^{-1} \right). \quad (34)$$

This completes the proof of Theorem 2.

### A.4 Scaling Analysis

For large  $N$ , expand the determinant:

$$\mathcal{C} = \frac{1}{2} \log \det \left( \frac{N\epsilon^2}{4} \Sigma^{-1} + I_k \right) \quad (35)$$

$$= \frac{1}{2} \log \left[ \left( \frac{N\epsilon^2}{4} \right)^k \det(\Sigma^{-1}) \cdot \det(I_k + O(1/N)) \right] \quad (36)$$

$$= \frac{k}{2} \log N + \frac{k}{2} \log \frac{\epsilon^2}{4} - \frac{1}{2} \log \det \Sigma + o(1). \quad (37)$$

Thus:

$$\boxed{\mathcal{C} = \frac{k}{2} \log N + O(1)}, \quad (38)$$

confirming that capacity grows logarithmically with query count  $N$  and linearly with projection dimension  $k$ .

### A.5 Relationship to Experiments

The capacity result provides an upper bound on the number of bits that can be reliably transmitted through the watermark channel. In our experiments, the message size is  $L = 5$  bits with  $k = 32$  and  $N = 4096$ . The observed statistical separation ( $> 8.4\sigma$ , Table 2) indicates that the empirical SNR is far above the threshold for reliable decoding of 5-bit messages. We do not experimentally probe the capacity upper bound (i.e., we do not test whether the  $\frac{k}{2} \log N$  scaling holds when the codebook size exceeds the orthogonal limit of  $k$  codewords). This remains as a direction for future work.

## B Watermark Persistence Under Extended Training

The 10K-step MNIST MLP results provide evidence that the watermark does not fade with extended training. Across all six watermarked models trained for 10,000 steps, detection accuracy remains 100%. The velocity loss decreases from  $\sim 0.41$  (at 5K steps) to  $\sim 0.37$  (at 10K steps), while the watermark correlation term stabilizes around 3.55–3.67 throughout the second half of training. This indicates that the two loss terms  $\mathcal{L}_{\text{vel}}$  and  $\mathcal{L}_{\text{wm}}$  reach a stable equilibrium: the model continues to improve its fit to the data distribution without suppressing the watermark signal. We attribute this to the structure of the watermark perturbation: since  $s_{K,m}(x,t)$  is orthogonal to the clean velocity field in expectation, the two objectives do not directly compete, and the watermark signal is maintained as a persistent offset in the learned dynamics.

The watermark correlation term stabilizes despite extended training (Table 2). The single false positive observed in the 10K-step clean model evaluation ( $1/40 = 2.5\%$ ) is below the random guess baseline of 3.1% and is not statistically significant after multiplicity correction.

## C Comparison with Existing Methods

Table 4: Comparison with existing generative model watermarking methods.

Method	Model-Level	Black-Box	Quality	Keyed	Multi-Bit
Tree-Ring [10]	✗	✓	✓	✓	✓
Stable Signature [5]	✓	✓	✓	Partial	✓
Weight embedding [9]	✓	✗	✗	✗	✓
Backdoor [1]	✓	✓	✗	✗	✗
BlackMarks [2]	✓	✓	✓	Partial	✓
<b>Ours</b>	✓	✓	✓	✓	✓

Table 4 summarizes how existing paradigms compare against the five desiderata. Our dynamics-level approach provides all five properties simultaneously. Two methods warrant additional discussion. Stable Signature [5] trains a decoder network alongside the generative model; the decoder weights serve as the key. Since the decoder is distributed with the model, anyone with model access has the key—the key is not an independent secret. BlackMarks [2] uses a secret trigger set for verification, providing keying through input-output behavior, though the triggers must remain confidential. Neither approach embeds the watermark at the level of continuous generative dynamics.

## D Capacity and Multiplexing

A natural question is whether message capacity can be increased beyond  $k$  bits by using multiple carrier frequencies (frequency-division) or time segments (time-division). We tested this empirically on MNIST and found that dividing the channel reduces per-carrier signal strength, degrading detection accuracy significantly compared to the single-carrier design.

The fundamental limitation is that dividing the channel among multiple carriers reduces the effective signal strength per carrier, as the total perturbation budget is shared.

Table 5: Multiplexing ablation on MNIST. Detection accuracy degrades when dividing the channel.

Method	Carriers/Segments	Bits	Accuracy
Single-carrier	1	5	100%
FDM-2	2	4	75%
FDM-4	4	12	75%
TDM-2	2	4	75%
TDM-4	4	12	58%

This lowers the per-carrier SNR and degrades detection accuracy, as observed in our experiments. We therefore adopt the single-carrier design. A rigorous study of multi-carrier random coding in this setting is left to future work.

## E Generated Samples

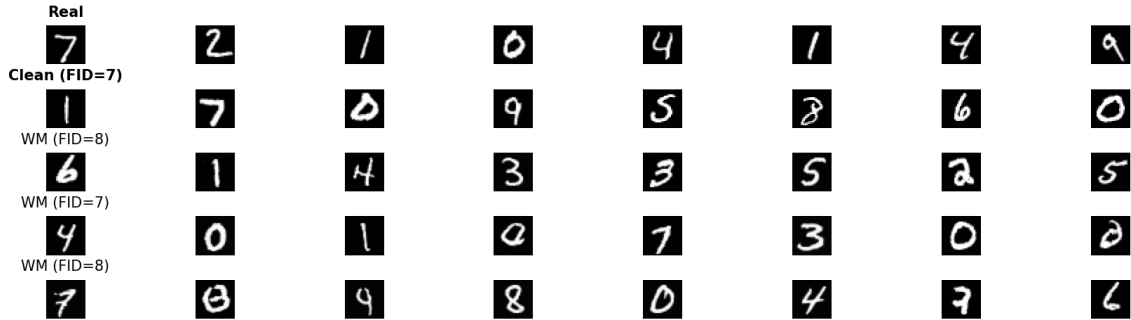


Figure 2: Generated MNIST samples from UNet + LoRA models. Top row: real MNIST digits. Second row: clean UNet model. Rows 3–5: watermarked LoRA models.

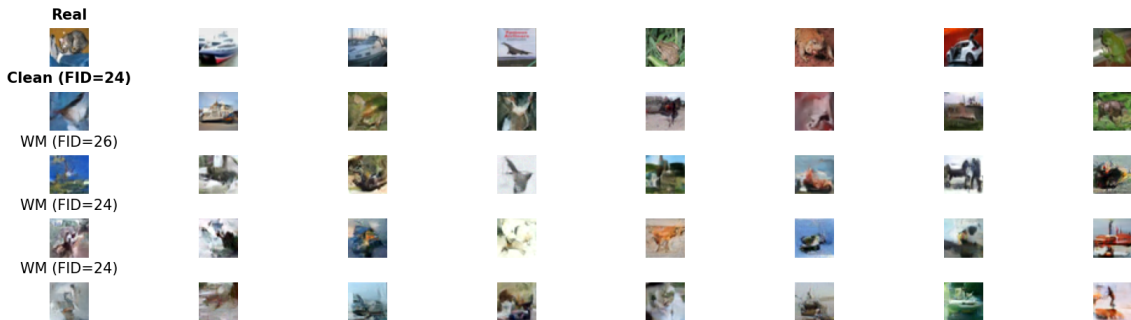


Figure 3: Generated CIFAR-10 samples from UNet + LoRA models. Top row: real CIFAR-10 images. Second row: clean UNet model. Rows 3–5: watermarked LoRA models.

## F Hyperparameters

Table 6: Complete hyperparameter configuration for all experiments.

Hyperparameter	MNIST (MLP)	MNIST (MLP 10K)	MNIST (UNet)	CIFAR-10 (UNet)
<i>Data</i>				
Image size	$28 \times 28$ (gray)	$28 \times 28$ (gray)	$28 \times 28$ (gray)	$32 \times 32$ (RGB)
Training samples	12,000	12,000	60,000	50,000
<i>Architecture</i>				
Model	4-layer MLP	4-layer MLP	UNet	UNet
Hidden size / ch.	1,024	1,024	64–256	64–256
Activation	SiLU	SiLU	SiLU	SiLU
LoRA rank	–	–	4	4
LoRA $\alpha$	–	–	8	8
<i>Flow Matching</i>				
Interpolation	Linear	Linear	Linear	Linear
Training steps (base)	5,000	10,000	5,000	5,000
Training steps (WM)	5,000	10,000	500 (LoRA)	500 (LoRA)
Batch size	512	512	512	512
Learning rate	$10^{-3}$	$10^{-3}$	$10^{-3}$	$10^{-3}$
Optimizer	AdamW	AdamW	AdamW	AdamW
<i>Watermark</i>				
Projection dim. $k$	32	32	32	32
Message bits $L$	5	5	5	5
Strength $\epsilon_0$	0.3	0.2	0.2	0.2
Loss weight $\lambda$	0.02	0.018	0.01	0.01
<i>Detection</i>				
Query budget $N$	4,096	4,096	4,096	4,096
Query distribution	$\mathcal{N}(0, 4I)$	$\mathcal{N}(0, 4I)$	$\mathcal{N}(0, 4I)$	$\mathcal{N}(0, 4I)$
Time sampling	Uniform(0, 1)	Uniform(0, 1)	Uniform(0, 1)	Uniform(0, 1)
<i>Evaluation</i>				
Watermarked models	6	6	3	3
Clean models	2	2	1	1
Trials per model	20	20	20	20